Journal of Physical Science, Vol. 33(3), 81–100, 2022

Calculating Microfield Angular Velocity Distribution in Plasma through Using Molecular Dynamics Simulation

Abdallah Bekkouche and Fethi Khelfaoui

University of Ouargla, Faculty of Mathematics and Material Sciences,
Radiation and Plasma and Surface Physics Laboratory, Ouargla 30000, Algeria

* Corresponding author: bekkouchabdallah@yahoo.fr

Published online: 30 November 2022

To cite this article: Bekkouche, A. & Khelfaoui, F. (2022). Calculating microfield angular velocity distribution in plasma through using molecular dynamics simulation. *J. Phys. Sci.*, 33(3), 81–100. https://doi.org/10.21315/jps2022.33.3.6

To link to this article: https://doi.org/10.21315/jps2022.33.3.6

ABSTRACT: *Considering the importance of statistics related to microfields in the spectral line shapes in plasma, many researchers were interested in calculating statistical distributions related to microfields with different models and approximations. Analytical approaches and numerical simulation methods can be used to study the variations of the magnitude or the directions of the microfield. The aim of this work is the calculation of distributions of microfield angles and distributions of microfield angular velocities on ions in plasmas. The article briefly presents an overview of previous work and the molecular dynamics simulation (MDS) technique used in this work. We consider interaction between all ions of the plasma according to Debye potential, and we follow evolution of the positions and velocities of particles according to Verlet algorithm. The results present effects of temperature and ion densities on calculated distributions. We compare our results with those of an analytical model based on Holtsmark model at the temperature* 10^5 *K, the ionic density* 2.10^{15} cm^{-3} *and for* $Z = +2$ *and* $Z = +5$*. Another comparison is done with independent particles model (IPM) for ionic coupling parameter equal to 0.17. Our values of the most probable angular velocity are less than those of the analytical calculation; differences may be caused mainly by the choice of the interaction potential and interaction between all ions in the plasma.*

Keywords: Debye potential, microfield angular velocities, molecular dynamics simulation, Holtsmark model, independent particles model

1. INTRODUCTION

To calculate the radiation spectrum in the plasma, we can exploit the microfield distribution, microfield derivative distribution, microfield correlation function and the microfield angle velocity distribution. The microfield is determined by the sum of elementary fields created by a very large number of elementary charges at a fixed charged or neutral point. Due to the difficulty of the analytical calculation of these functions, numerical simulation methods can be used. Several authors have been interested in the study of these distributions; we quote below the works of some authors:

Smith and Hooper improved the shape of the line of radiative transition between the center of the line and the wings of the line by using the extended ionised microfield function.[1] Gasparyan et al. studied the multi-charged ions in the plasma considering the influence of the electric microfield both on the shape of the spectral line and on the dynamics of the atomic system.[2] The density matrix formalism was employed. Kilcrease et al. presented a formalism for the calculation of the low frequency electric microfield at a charged point in a plasma; they investigated the validity of the two-temperature plasma model as well as the impact of this microfield on the first three members of the Lyman emission line series of hydrogenic aluminum.[3] Murillo et al. examined multiple approaches for computing plasma microfield-constrained-average quantities; these quantities were performed in the context of microfield restricted field gradients, and they are used to describe the ion quadruple effect.[4] To determine the microfield distribution function of the ion component, Ramazanov et al. used the Iglesias approach; the distribution function is precisely stated in terms of a two-body function.[5] Iglesias et al. were able to compute the distribution of fast electric microfields in extreme matter conditions, they used the adjustable parameter exponential approximation (APEX) to represent microfield at large fields from the nearest neighbor.[6] Benbelgacem et al. used the Baranger–Mozer approximation theory to compute the microfield distribution in two-component plasmas. They employed the fixed-point approach and the Runge–Kutta method to solve the integral equation of the effective potential energy.[7] In a two ionic component plasma (TICP), Meftah et al. estimated the autocorrelation function for the velocity and electric microfield of an impurity ion; then they assumed the provided approximation to have a disconnected one to the collision operator.[8] Douis and Meftah calculated classical and relativistic electric field autocorrelation function according to an integral equation for an effective potential energy; the interaction is taken at first time as screened Deutsh interaction and at the second time as Kelbg interaction.[9] Approximations to the limited electric microfield gradient joint probability distribution function were investigated by Kilcrease and Murillo; they described the probability of specific field gradients for a given plasma microfield value. The analytic approximations based on the APEX microfield description were employed, as well as the molecular dynamics simulation (MDS) approach.[10] Guerricha et al. determined the spatial derivative of components of the quasistatic ion electric microfield in plasma; the independent particles model (IPM) was employed.[11] Chenini et al. computed the distribution functions of the spatial derivative ion microfield distributions using the Monte Carlo Simulation (MCS) method; these distributions were used to demonstrate the asymmetry of the Lyman-line in He+ plasma.[12] Calisti et al. examined effect of dynamic microfield by studying the effects of two electric field models.[13] The first model is a pure rotating field with constant magnitude; the second is a model of a time-dependent magnitude field in a given direction. They discussed the effects of a time-dependent ionic field on the shapes of the He+ Lyman-lines for various densities and temperatures.

Demura reviewed the current status of microfield, a process which has been successful and profitable for experimental and theoretical studies of plasma in both gas discharges, and thermonuclear modeling installations for many decades, he also described the concepts of the microfield models that have been used.[14] The review presents, for both analytical, numerical and simulation models, distributions of microfield, pair radial distribution (or pair radial correlation function) and time microfield autocorrelation functions.

In other works, Demura and Stambulchik, and also Stambulchik and Demura, investigated the effect of microfield fluctuations on Stark profiles in the perturbative approach to ion dynamics for the Theory of Thermal Corrections (TTC); they used the effects of ion dynamics which induce microfield fluctuations caused by rotations. Using non-perturbative computer simulations, results show that the Stark profiles in the line center were within TTC expectations.[15,16]

Adaika and Meftah used the Holtsmark model to determine the angular velocity distribution of the electric microfield while keeping its strength constant and equal to its value.[17] They used the Holtsmark approach and the IPM to compute the static distribution functions of the angular velocity of the microfield. They used the obtained static distributions to show the effect on the broadening of Lyman-alpha line for plasma composed of He^+ ions.

The shape of spectral lines in plasmas can be affected by ion dynamics; the analytical approaches suggest studying the variations of the magnitude or the directions of the microfield on an ion (or atom) during the emission of the radiation. In this article, we calculate the angles distributions of microfield on ions, their microfield angular velocity and effects of density and temperature on these distributions. We compare our results with those of Adaika and Meftah work.

This paper consists of four sections. The introduction contains the importance and the purpose of the study, with previous works and research. Section two highlights the objective of MDS and our calculation method. In the third section, we highlight the results then the most important findings; adding to their behavior with plasma media temperatures and densities. Conclusion appears in section four.

2. MOLECULAR SIMULATION DYNAMICS

2.1 Objectives of the MDS simulation

Molecular dynamics is a numerical method for studying many-particle systems such as molecules, clusters and even macroscopic systems such as gases, liquids and solids. It is used extensively in materials science, chemical physics, biophysics and biochemistry. MDS follows the detailed motion of sets of interacting atoms through the integration of the atomic equations of motion throughout the use of inter-atomic potentials. MDS aims at understanding the properties of assemblies of molecules in terms of their structures, and the microscopic interactions between them. This simulation is a complement to conventional experiments, and could treat comparatively; large systems for a relatively long time. It helps interpret experiments and provide alternative interpretations; it also, gives detailed molecular-level information which enables us to learn something new that cannot be found by other methods. In our topic, the assumption is made of plasma with velocities according to Maxwell-Boltzmann distribution; the temperature is constant. The electrons are considered as a continuous depth with ions interactions according to Debye potential.

2.2 Simulation initialisation

The simulation program begins by reading the numerical and physical quantities needed for the calculation. The program calculates plasma parameters: Debye length $\lambda_{D,\,ion}$ic plasma frequency ω_P, ionic coupling parameter Γ_{ii} and sphere radius R_i, which are defined below. All equations of this paper are written in centimeter-gram-second (CGS) units.

$$\lambda_D = 6.9\left(\frac{T}{Z\ n_i}\right)^{1/2} \tag{1}$$

Where T is the temperature, n_i is the density of ions and Z is the charge number of the ion.

$$\omega_p = \left(4\pi (Z\ e)^2 \frac{n_i}{m_i}\right)^{1/2} \tag{2}$$

Where e is the electron charge and m_i is the mass of an ion.

$$R_i = \left(\frac{3}{4\pi n_i}\right)^{1/3} \tag{3}$$

$$\Gamma_{ii} = \left(\frac{(Z\ \ e)^2}{k_B T R_i}\right) \tag{4}$$

Where k_B is the Boltzmann constant.

2.3 Basic Principles and Verlet Algorithm for MDS

A good reference on some basic principles of MDS is the work of Hansen and Mc Donald.[18]

We choose a cubic cell that contains N ions. The length of the side of the cell is related to the ionic density and the number of ions in it. The choice of the value of N must respond to the convergence of the results of the simulation.

Let be the vector of the position of an ion i; and let be a vector between two ions i and j. The force between two ions derives from the Debye potential (screened Coulomb potential) V(r).

$$V(r) = \frac{Ze}{r_{ij}} \exp\left(-\frac{r_{ij}}{\lambda_D}\right) \tag{5}$$

To calculate the sum of the forces applied to an ion, we centered the cell around the ion. We take the total force on the ion according to the equation:

$$\vec{F_i} = \Sigma_{\mathrm{j}\neq\mathrm{i}}^{\mathrm{N}-1} \left(\frac{(Ze)^2}{r_{ij}^3}\right)\left(\frac{1+r_{ij}}{\lambda_D}\right)\exp\left(-\frac{r_{ij}}{\lambda_D}\right)\vec{r_{ij}} \tag{6}$$

The principle of the MDS is the resolution of equations of motion of ions in the simulation cell.

For the first step of the simulation method, at the initial moment t = 0, we randomly distribute the position of the ions in the cubic cell and the velocities of the ions. Using RANDOM generator of real numbers, the positions are distributed as uniform law and velocities are distributed according to the Maxwell Boltzmann distribution.

For the second step of the simulation method, we calculate positions of ions at time t = Dt as follow:

$$\vec{r_l}(\Delta t) = \vec{r_l}(0) + \Delta t\, \vec{v_l}(0) + (\Delta t)^2 \textstyle\sum_{i \neq j} \vec{F_{ij}}(0) / 2m_i \qquad (7)$$

For the following steps, we calculate the evolution of ion positions and velocities by the Verlet algorithm.

$$\vec{r_l}(t+\Delta t) = 2\vec{r_l}(t) + \vec{r_l}(t-\Delta t) + (\Delta t)^2 \textstyle\sum_{j \neq i} \vec{F_{ij}}(t) / m_i \qquad (8)$$

$$\vec{v_l}(t) = (\vec{r_l}(t+\Delta t) - \vec{r_l}(t-\Delta t)) / (2\Delta t) \qquad (9)$$

Two conditions are too important for the evolution of the simulation: (1) the choice of the time step Δt and (2) the boundary conditions at the edges of the cell.

1. The time step Δt can be taken of the order of Δt = T/100 (or less), as generally the free ion oscillations are with the plasma frequency $\omega_{p;}$ where $T = 2\pi/\omega_p$ is the period of oscillation related to ionic plasma frequency.

2. To minimise the surface effect, periodic boundary conditions (PBC) is used. The ions that we follow are in the central cell; if an ion crosses a wall with a certain velocity, its image returns with the same velocity by the opposite wall. Under these conditions, the number of particles in the cell, and consequently the density, is constant. These conditions also allow the conservation of the energy and the momentum of the system and do not introduce periodic effects (because of the interaction between ions).[18]

Once the equations of motion have been solved, we can take and calculate the different averages and statistics. In this work, the study is on the microfield properties. For a non-relativistic motion, the microfield on an ion is easily deduced from the force:

$$\vec{E} = \vec{F_l} / Ze \qquad (10)$$

We calculate the angles α between the microfield and the velocity vector of the curvy linear coordinates and angles with axes of Cartesian plan (θ_x, θ_y, θ_z) for each ion. The angle α is necessary for determining angular velocity w_α; it also allows to determine the tangential component and the normal component of the microfield and the radius of curvature for a path of the ion. Figure 1 shows angle α between the velocity vector and the microfield. Figure 2 shows angles θ (for θ_z) and φ in the Cartesian plane for microfields. The following equations are those of the angles:

$$\alpha = arcos\left((v_{ix}E_x + v_{iy}E_y + v_{iz}E_z) / |\vec{v_l}||\vec{E}|\right) \qquad (11)$$

Where v_{ix}, v_{iy}, v_{iz} are the components of the velocity and E_x, E_y, E_z are the components of the microfield.

$$\theta_x = arcos\left(E_x / |\vec{E}|\right) \tag{12}$$

$$\theta_y = arcos\left(E_y / |\vec{E}|\right) \tag{13}$$

$$\theta_z = arcos\left(E_z / |\vec{E}|\right) \tag{14}$$

$$\varphi = arcos\left(E_x / E_y\right) \tag{15}$$

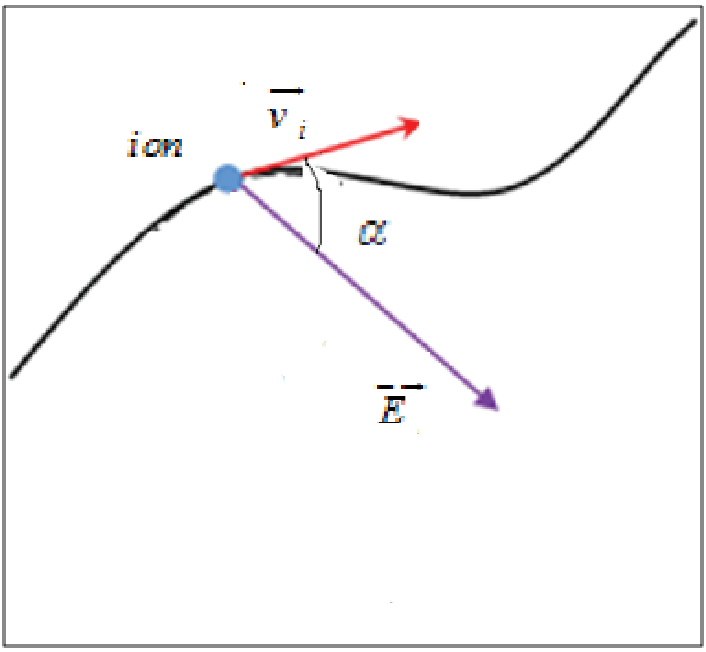

Figure 1: Angle α between the microfield and the velocity vector.

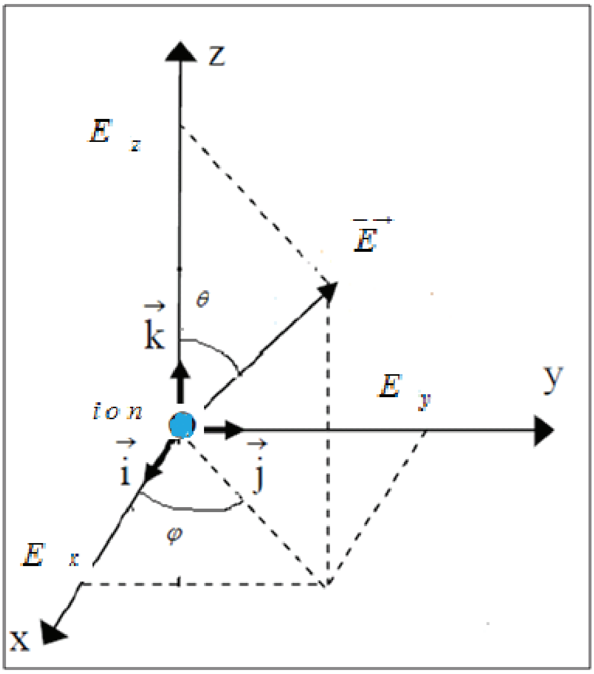

Figure 2: Angles θ and φ in the Cartesian plane for microfields.

We deduce temporal derivatives of angles w_α, w_x, w_y, w_z, w_φ, and magnitude (modulus) of angular velocity of the electric microfield ω as follows:

$$\omega_x = \left(\frac{\Delta\theta_x}{\Delta t}\right) \tag{16}$$

$$\omega_y = \left(\frac{\Delta\theta_y}{\Delta t}\right) \tag{17}$$

$$\omega_z = \left(\frac{\Delta\theta_z}{\Delta t}\right) \tag{18}$$

$$\omega_\alpha = \left(\frac{\Delta_\alpha}{\Delta t}\right) \tag{19}$$

$$\omega_\varphi = \left(\frac{\Delta\varphi}{\Delta t}\right) \tag{20}$$

$$\omega = (\omega_x^2 + \omega_y^2 + \omega_z^2)^{1/2} \tag{21}$$

As our plasma medium is homogeneous in stationary state, we calculate statistics of values on all ions and at many time steps. Our medium is also isotropic; the directions of the x, y and z axes are equivalent and therefore the statistics on the angles θ_x, θ_y and θ_z are equivalent.

3. RESULTS AND DISCUSSION

We consider a plasma essentially formed of hydrogen-like argon ions, with: $Z = +17$ and $m_i = 40$ amu (amu = atomic mass unit). We calculate distributions of angles of microfields and temporal derivatives distribution for these angles for different temperature sand densities. The surfaces of the calculated curves (distributions) are normalised to unity in the computational domain. For numerical results, we consider number of particles in cell $N = 54$. Time step Δt is taken about T/1000, this time step makes it possible to follow the variations of the requested angular velocities.

3.1 Distribution of Microfield Angles

Figures 3 and 4 present a parametric study of the distribution of microfield angles $P(\alpha)$ for different values of densities and temperatures. The curves are presented in the domain (1.56rad, 1.58rad), which presents a difference of 0.02 rad = 1° around $\pi/2 = 90°$. Under these conditions, the microfield can be considered to be practically normal to the trajectory (in terms of probability). The curves of these distributions are symmetrical with respect to the value $\pi/2$, which corresponds to the most probable value $\alpha^* = \pi/2$. In figure 3, for the same temperature $T = 10^7$ K, the values of the probability of the most probable angle ($\alpha^* = \pi/2$) decrease when the density increases; the curves become wider. In Figure 4, for the same density $n_i = 10^{19}$ cm^{-3}, also the values of the probability of the most probable angle ($\alpha^* = \pi/2$) decrease when the temperature increases; the curves become wider.

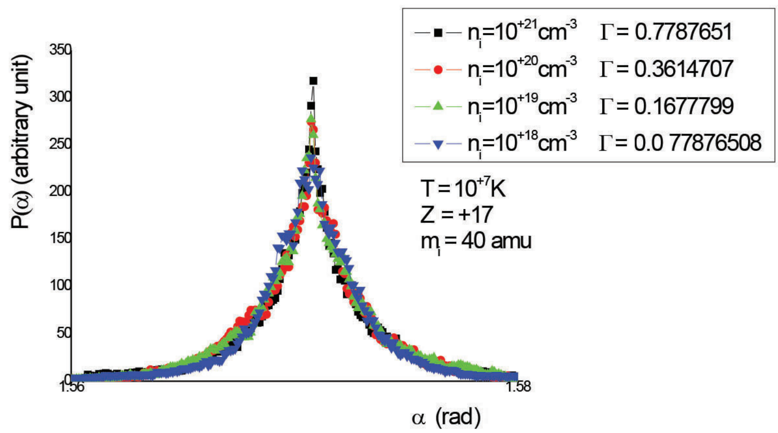

Figure 3: Distribution P(α) for different values of densities.

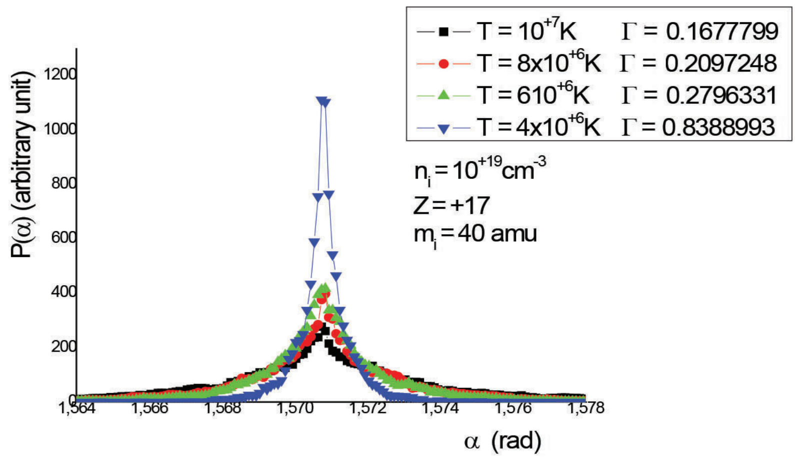

Figure 4: Distribution P(α) for different values of temperatures.

Figure 5 presents the distribution P(θ) of the angle θ. It is symmetric with respect to the value π/2 and it is not sensitive to values of densities and temperatures. The calculation of the distribution of cos(θ) shows that it has a constant value.

The calculation shows, also, that the distribution P(φ) of the angle φ has a constant value in the domain [0, 2p].

The P(θ) and P(φ) distributions confirm the equiprobability of the directions of the electric microfield in space. This property is used in the calculation of microfield distributions in several works, it is considered as a static property in plasma spectroscopy. The distribution of microfield angles P(α), of the angle α in the moving coordinate system of the ion, depends on the collision conditions (velocities, temperatures and densities).

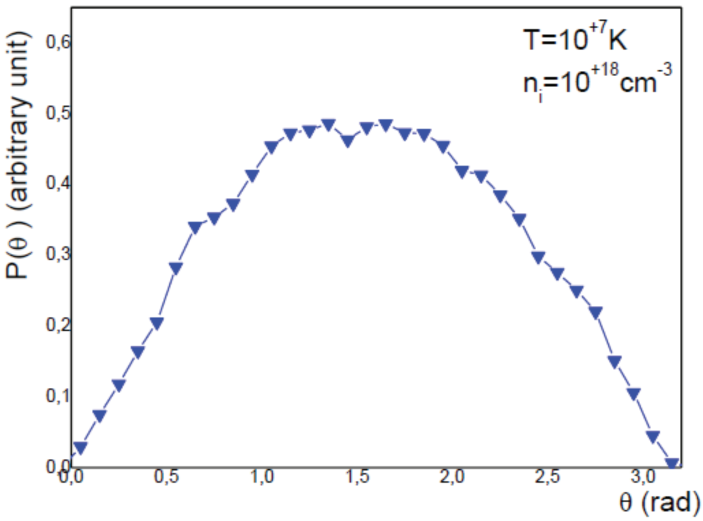

Figure 5: Distribution P(θ) of the angle θ.

3.2 Distribution of Temporal Derivatives of Microfield Angles

Figures 6 and 7 present a parametric study of the distribution $P(\omega_\alpha)$ of temporal derivative of microfield angle α for different values of densities and temperatures. The curves of these distributions are not symmetrical with respect to the axis $\omega_\alpha = 0$, which corresponds to the most probable value $\omega_\alpha^* = 0$. In Figure 6, for the same temperature $T = 10^7$ K, the values of the probability of the most probable angular velocity ($\omega_\alpha^* = 0$) decrease when the density increases; the curves become wider on the side of negative values. In Figure 7, for the same density $n_i = 10^{24}$ cm^{-3}, also the values of the probability of the most probable angular velocity ($\omega_\alpha^* = 0$) decrease when the temperature increases; the curves become wider on the side of negative values. For $T = 10^7$ K and $n_i = 10^{19}$ cm^{-3}, and for a probability equal to half that of the most probable value, the curve is wider by 97% on the left side than on the right side (compared to ω_α^*). In Figure 7, high temperatures show more the dominance of negative values of ω_α.

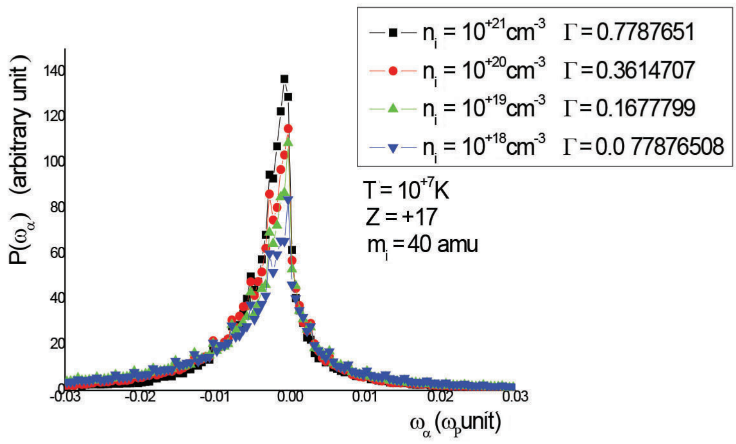

Figure 6: Distribution $P(\omega_\alpha)$ for different values of densities.

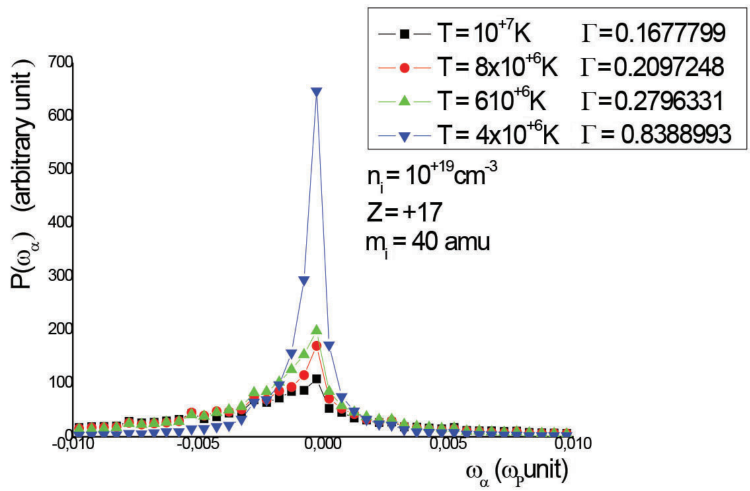

Figure 7: Distribution $P(\omega_\alpha)$ for different values of temperatures.

Figures 8 and 9 present a parametric study of the distribution $P(\omega_\theta)$ of temporal derivative of microfield angle θ for different values of density and temperature. The most probable value is $\omega_\theta^* = 0$, it increases to higher densities (Figure 8) and it decreases (Figure 9) at higher temperature. This result is in agreement with that of the literature.[17] The different curves are symmetrical with respect to the $\omega_\theta^* = 0$ axis.

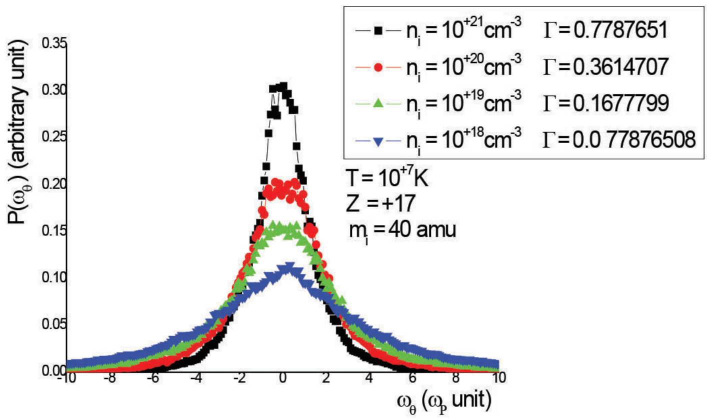

Figure 8: Distribution $P(\omega_\theta)$ for different values of densities.

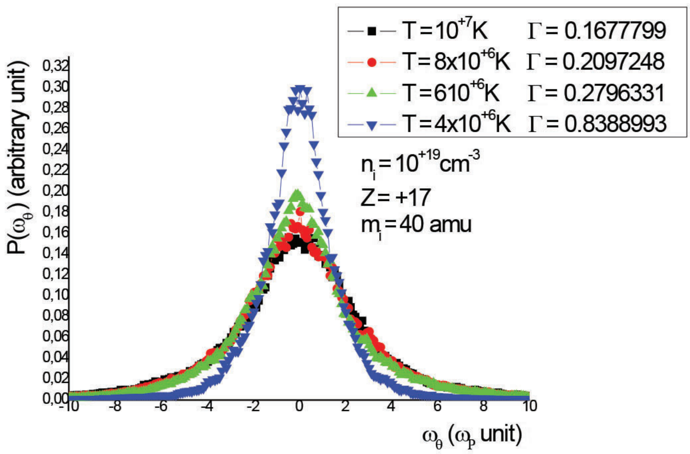

Figure 9: Distribution $P(\omega_\theta)$ for different values of temperatures.

Figures 10 and 11 represent a parametric study of the distribution $P(\omega_\varphi)$ of temporal derivative of microfield angle φ for different values of density and temperature. The most probable value is $\omega_\varphi^* = 0$, it increases at higher densities (Figure 10) and it decreases (Figure 11) at higher temperatures. The different curves are symmetrical with respect to the $\omega_\varphi^* = 0$ axis. In contrary to $P(\omega_\alpha)$, the $P(\omega_\theta)$ and $P(\omega_\varphi)$ distributions have significant widths in ω_p unit.

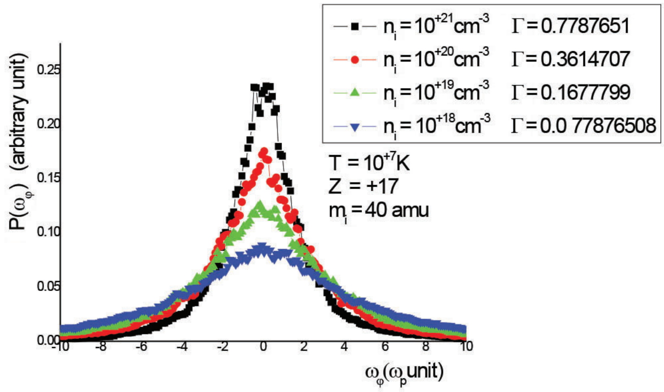

Figure 10: Distribution $P(\omega_\varphi)$ for different values of densities.

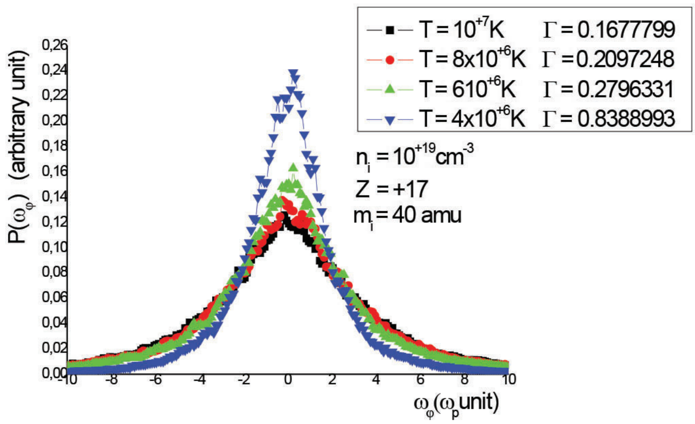

Figure 11: Distribution P (ω_φ) for different values of temperatures.

3.3 Angular Velocity Distribution of the Electric Microfield

In this sub-section, we are interested to calculated the distribution P(ω) of the magnitude of angular velocity ω of the electric microfield according to the equation (21). We compare also our result with some results of work of Adaika and Meftah published in 2014. They used analytical approaches respecting the Holtsmark model and the IPM.[17]

Figure 12 represents the effect of density on angular velocity distribution P(ω), for ions of Z = +17, $m_i = 40$ amu and at temperature $T = 10^7$ K. We observe a decrease in the value ω* (in ω_p unit) of the most probable angular velocity ω* decreases when density increases. Thermal velocities having the same values, with increasing density, the coupling parameter Γ_{ii} increases (despite the screen effect decrease) and the electrostatic effect increases. The angular velocities of the electric fields become smaller (in ω_p unit). The ratio ω_1*/ω_2* between the two values of $\omega*$, in ω_p unit, is about 1.68 for densities $n_{i1} = 10^{18}$ cm^{-3} and $n_{i2} = 10^{20}$ cm^{-3}; in absolute unit (s), this ratio is 16.8.

Figure 13 represents the effect of temperature on angular velocity distribution $P(\omega)$, for the same ions ($Z = +17$, $m_i = 40$ amu) and at density $n_i = 10^{19}$ cm^{-3}. We observe an increase in the value of $\omega*$ when temperature increases. Under these conditions, the unit of time being the same (in unit ω_p), the average distance R_i between ions is the same (despite the screening effect increasing) and the velocities of the ions in the plasmas become greater with the increase in temperature. The angular velocities ω become larger.

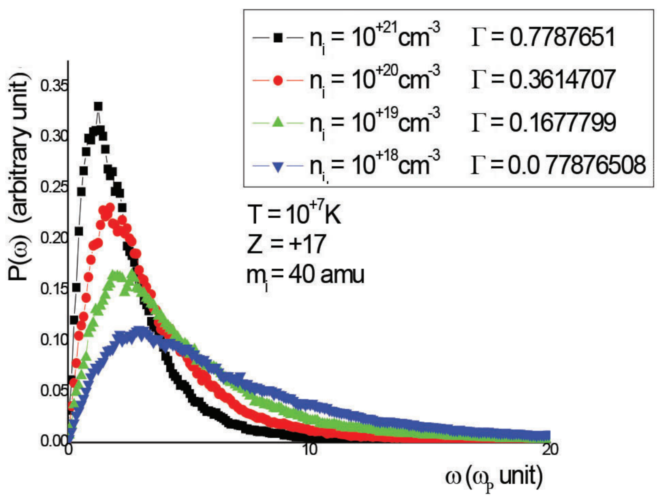

Figure 12: Angular velocity distribution $P(\omega)$ for different values of densities.

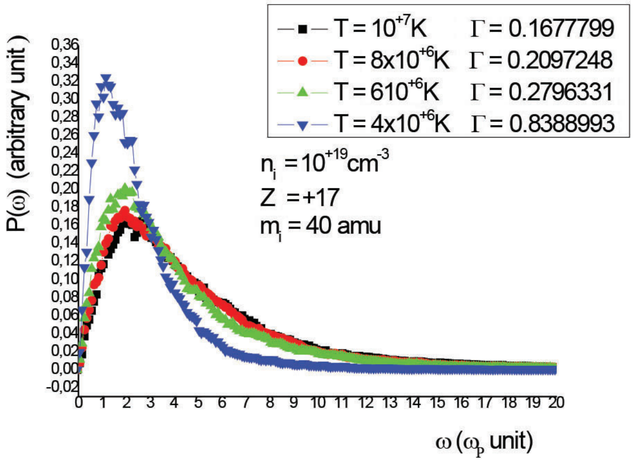

Figure 13: Angular velocity distribution P(ω) for different values of temperatures.

Figures 14 and 15 present a comparison of the microfield angular velocity distribution P(ω) with Holtsmark model used in Adaika and Meftah work for $T = 10^5$ K, $n_i = 2.10^{15}$ cm^{-3}, and for Z = +2 and Z = +5. We take $m_i = 12$ amu, our calculation gives values ω* (or $(\omega^*)_{MDS}$) of the most probable angular velocity less than those of the analytical calculation $(\omega^*)_{Hol}$. The ratios $(\omega^*)_{MDS}/(\omega^*)_{Hol}$ between the two calculations are about 0.46 for Z = +2 and 0.68 for Z = +5. Differences may caused mainly by the fact that our calculation takes into account the interaction with Debye potential of all the ions with the target ion, and the interactions between all the ions between them. In addition, in MDS it is a more or less exact resolution of the equation of motion.

In same work, they done another calculation using the IPM for $\Gamma_{ii} = 0.17$; for the most probable value for IPM $(\omega^*)_{IPM} = 4.00$ (in w_p unit) and the most probable value for Holtsmark model $(\omega^*)_{Hol} = 5.09$ (in w_p unit), the ratio $(\omega^*)_{IPM}/(\omega^*)$Hol is about 0.78.[17] Our calculation with MDS gives $(\omega^*)_{MDS} = 2.85$ (in w_p unit), for $\Gamma_{ii} = 0.17$, $T = 2.10^4$ K, $n_i = 2.10^{18}$ cm$^{-3,}$ Z = +1 and $m_i = 40$ amu; so the ratio $(\omega^*)_{MDS}/(\omega^*)$ IPM is about 0.71. Figure 16 shows the distributions P(ω) for Holtsmark model, IPM and MDS; IPM results are closest to those of MDS.

For the Holtsmark model, it was demonstrated that $P(w_\theta)$ has a Lorentzian distribution; and the calculated distribution P(ω) is a sum of two functions.[17] The final profile is a sum of two components. In the same work, it was highlighted that $P(\omega_\theta)$ has a Gaussian distribution for IPM. Further study by the MDS will make it possible to see the shape of the elementary components along the axes and the final composition of the distributions.

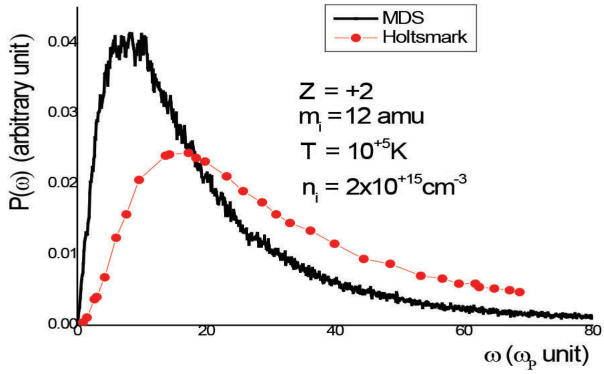

Figure 14: Comparison of the angular velocity distribution P(ω) with the Holtsmark model for Z = +2.

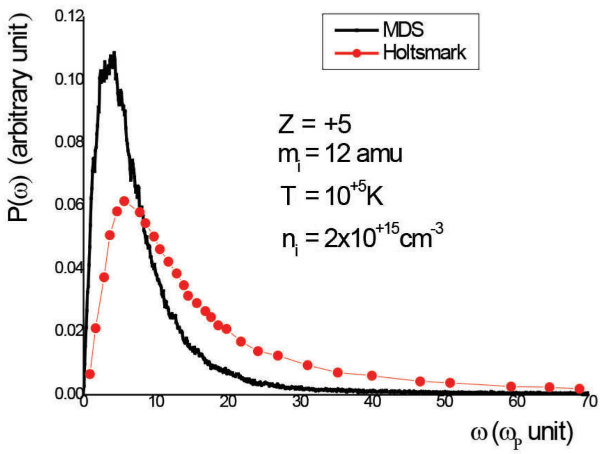

Figure 15: Comparison of the angular velocity distribution P(ω) with the Holtsmark model for Z = +5.

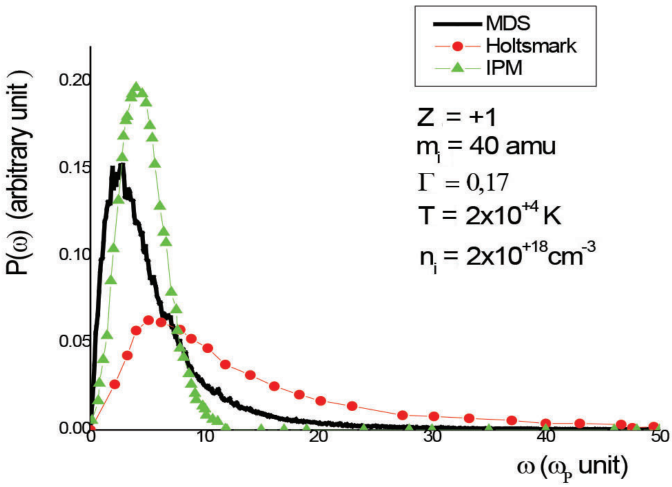

Figure 16: Comparison of the angular velocity distribution P(ω) with IPM and Holtsmark model for $\Gamma_{ii} = 0.17$.

4. CONCLUSION

As far as, research on the effect of the dynamics of ions on the shape of spectral lines is concerned, among other things, with the influence of the directionality of the ionic field. In this paper, we highlighted calculations of microfield angular velocity distributions on an ion in plasma using the MDS model. In the calculation method, all the ions interact with each other according to a screened Debye potential, and the equations of motion are solved in the simulation cell. We calculate the distributions of microfield angles and the distributions of temporal derivatives of angles on ions (Z = +17). For the microfield angle α, the most probable value is $w_\alpha^* = 0$, and its probability depends on the values of the densities and the temperatures. The distribution is not symmetrical; the curve becomes wider on the side of negative values of w_α. At high temperatures, there is more dominance of negative values of w_α. We also compute the distribution P(ω) of the magnitude of the electric microfield's angular velocity ω. For $T = 10^5$ K and $n_i = 2.10^{15}$ cm^{-3}, we compare our results with those of the Holtsmark model; the ratios between the values of ω* are 0.46 and 0.68 for Z = +2 and Z = +5, respectively. For $\Gamma_{ii} = 0.17$, the comparison with the IPM calculation gives a ratio of 0.71. Our values of the most probable angular velocity are less than those of the analytical calculation. Differences may be caused mainly by the fact that our calculation takes into account the Debye potential of all the ions between them. As a prospect, it would be interesting to study the angular velocity distribution of the microfield for plasma with several ionic species and study the effect of microfield angular velocities on spectral line shapes.

5. ACKNOWLEDGEMENTS

The authors acknowledge the support of the LRPPS Laboratory, University of Ouargla, General Directorate of Scientific Research and Technological Development (DGRSDT), and the Agency for Thematic Science and Technology Research (ATRST).

6. REFERENCES

1. Smith, E. W. & Hooper, C. F. (1968). Comments on ion microfield distributions as used in plasma line broadening theories. *J. Quant. Spectrosc. Radiat. Transf.*, 8(9), 1617–1619. https://doi.org/10.1016/0022-4073(68)90056-3
2. Gasparyan, P. D. et al. (1994). Effect of plasma microfields on the gain of hydrogen-like ions with photoresonant pumping. *In the Intermission*, 105, 1593–1605. https://doi.org/10.1142/9789812815941_0030
3. Kilcrease, D. P. (1994). Plasma electric microfields for differing electron and ion temperatures. *J. Quant. Spectrosc. Radiat. Transf.*, 51(1–2), 161–167. https://doi.org/10.1016/0022-4073(94)90076-0
4. Murillo, M. S. et al. (1997). Dense plasma microfield nonuniformity. *Phys. Rev. E*, 55, 6289–6292. https://doi.org/10.1103/PhysRevE.55.6289
5. Ramazanov, T. S. et al. (2012). Microfield distribution in semiclassical plasma. *Int. J.l Math. Phys.*, 3(2), 140–143.
6. Iglesias, C. A. et al. (2000). Fast electric microfield distribution calculations in extreme matter conditions. *J. Quant. Spectros.*, 65(1–3), 303–315. https://doi.org/10.1016/S0022-4073(99)00076-X
7. Benbelgacem, K. et al. (2017). Effect of electron – ion coupling on the electric microfield distribution in plasmas. *Contrib. Plasma Phys.*, 57(4), 176–181. https://doi.org/10.1002/ctpp.201700005
8. Meftah, M. T. et al. (2004). Electric field dynamics at charged point in two component plasma. *Eur. Phys. J. B*, 37, 39–46. https://doi.org/10.1140/epjb/e2004-00028-x
9. Douis, S. & Meftah, M. T. (2013). Correlation function and electronic spectral line broadening in relativistic plasmas. *Serb. Astron. J.*, 186, 15–23 https://doi.org/10.2298/SAJ130218002D
10. Kilcrease, D. P. & Murillo, M. S. (2000). The ion electric microfield gradient joint probability distribution function for dense plasmas. *J. of Quant. Spectrosc. Radiat. Transf.*, 65(1–3), 343–352. https://doi.org/10.1016/S0022-4073(99)00079-5

11. Guerricha, S. et al. (2012). Distribution function of spatial derivative of the ion electric microfield using the independent particles model in plasmas. *Contrib. Plasma Phys.*, 52(9), 776–783. https://doi.org/10.1002/ctpp.201200026
12. Chenini, K. et al. (2011). Contribution to calculation of ion microfield nonuniformity effect on the asymmetry of Lyman-α line in dense plasma. *Contrib. Plasma Phys.*, 51(1), 34–43. https://doi.org/10.1002/ctpp.201000025
13. Calisti, A. et al. (2014). Influence of microfield directionality on line shapes. *Atoms*, 2(2), 259–276. https://doi.org/10.3390/atoms2020259
14. Demura, A. V. (2010). Physical Models of Plasma Microfield. *Int. J. Spectros.*, 2010, 1–42. https://doi.org/10.1155/2010/671073
15. Demura, A. V. & Stambulchik, E. (2014). Spectral-kinetic coupling and effect of microfield rotation on stark broadening in plasmas. *Atoms*, 2(3), 334–356. https://doi.org/10.3390/atoms2030334
16. Stambulchik, E. & Demura, A. V. (2015). Ion dynamics and effects of microfield rotation. Paper presented at the *X Serbian Conference on Spectral Line Shapes in Astrophysics*, Srebrno jezero, Serbia, 15–19 June 2015, 68–68.
17. Adaika, H. & Meftah, M. T. (2014). Angular velocity distribution of the electric microfield in plasma. *Contrib. Plasma Phys.*, 54(7), 669–679. https://doi.org/10.1002/ctpp.201300041
18. Hansen, J. P. & Mc Donald, I. R. (1976). *Theory of Simple Liquids*. London: Academic Press, 428p.